

# ULRR

## Experimental modelling of aortic aneurysms: novel applications of silicone rubber

Item Type	Article
Authors	Doyle, Barry J.;Corbett, Timothy J.;Walsh, Michael;Cloonan, Aidan J.;O'Donnell, Michael R.;Vorp, David A.;McGloughlin, Timothy M.
Citation	Medical Engineering & Physics;31/8/1002-1012
Publisher	Elsevier
Download date	2026-06-10 12:52:49
Item License	<a href="https://creativecommons.org/licenses/by-nc-sa/1.0/">https://creativecommons.org/licenses/by-nc-sa/1.0/</a>
Link to Item	<a href="https://hdl.handle.net/10344/205">https://hdl.handle.net/10344/205</a>

# **EXPERIMENTAL MODELLING OF AORTIC ANEURYSMS: NOVEL APPLICATIONS OF SILICONE RUBBERS**

Barry J. Doyle<sup>1§</sup>, Timothy J. Corbett<sup>1</sup>, Aidan J. Cloonan<sup>1</sup>, Michael R. O'Donnell<sup>1</sup>,  
Michael T. Walsh<sup>1</sup>, David A. Vorp<sup>2</sup> and Timothy M. McGloughlin<sup>1</sup>

1. Centre for Applied Biomedical Engineering Research (CABER), Department of Mechanical and Aeronautical Engineering, and Materials and Surface Science Institute, University of Limerick, Ireland.
2. Departments of Surgery and Bioengineering, Centre for Vascular Remodeling and Regeneration, McGowan Institute for Regenerative Medicine, University of Pittsburgh, USA.

## ABSTRACT

### Background

A range of silicone rubbers were created based on existing commercially available materials. These silicones were designed to be visually different from one another and have distinct material properties, in particular, ultimate tensile strengths and tear strengths.

### Methods

In total, eleven silicone rubbers were manufactured, with the materials designed to have a range of increasing tensile strengths from approximately 2-4 MPa, and increasing tear strengths from approximately 0.45-0.7 N/mm. The variations in silicones were detected using a standard colour analysis technique. Calibration curves were then created relating colour intensity to individual material properties. All eleven materials were characterised and a 1<sup>st</sup> order Ogden strain energy function applied. Material coefficients were determined and examined for effectiveness. Six idealised abdominal aortic aneurysm models were also created using the two base materials of the study, with a further model created using a new mixing technique to create a rubber model with randomly assigned material properties. These models were then examined using videoextensometry and compared to numerical results.

### Results

Colour analysis revealed a statistically significant linear relationship ( $P < 0.0009$ ) with both tensile strength ( $R^2 = 0.8082$ ) and tear strength ( $R^2 = 0.7205$ ), allowing material strength to be determined using a non-destructive experimental technique. The effectiveness of this technique was assessed by comparing predicted material properties to experimentally measured methods, with good agreement in the results. Videoextensometry and numerical modelling revealed minor percentage differences, with all results achieving significance ( $P < 0.0009$ ).

### Conclusions

This study has successfully designed and developed a range of silicone rubbers that have unique colour intensities and material strengths. Strengths can be readily determined using a non-destructive analysis technique with proven effectiveness. These silicones may further aid towards an improved understanding of the biomechanical behaviour of aneurysms using experimental techniques.

## INTRODUCTION

Silicone is a synthetic polymer consisting of a linear backbone of repeating, alternating silicone and oxygen atoms. Each silicone atom has two groups attached to it, referred to as R groups, representing any organic group that may be attached to the backbone. This structure forms a polymer called polydimethylsiloxane (PDMS), and is the most commonly used silicone. Rubber-like materials are comprised of very long-polymeric chains united by vulcanisation into a network structure. These rubbers can therefore undergo large recoverable deformations, hence the wide use of silicone rubbers as material analogues in the study of arterial vessels<sup>1-4</sup> and other soft tissues.<sup>5</sup> At high strain rates, similar to those naturally found within the cardiac cycle, polymeric chain deformation is usually restricted to bending and stretching of the chemical bonds within the network. As a result the storage modulus of the rubber can increase by up to three orders of magnitude.<sup>5</sup> Abdominal aortic aneurysms (AAA) are permanent irreversible dilations of the infrarenal section of the aorta, and will eventually expand to the point of rupture if left untreated. Many previous studies have focussed on the numerical prediction of wall stresses and ultimately rupture prediction of AAAs.<sup>6-15</sup> However, there has been limited reports as to how these aneurysms behave experimentally,<sup>2,17,18</sup> in particular, how these models react to increased pressure loadings above the average peak systolic pressure of 120 mmHg. Also, previous experimental work has employed the use of a single material to represent the AAA wall, even though it is known that a realistic AAA may have differing material properties at various locations throughout the aneurysm.<sup>19</sup>

The primary aim of this study was to develop a range of silicones of known colour and known material properties. Commercially available silicone was used in conjunction with a method of colour analysis in order to develop calibration curves. These calibration curves consist of a direct relationship between material colour and both tensile strength and tear strength. Material characterisation was determined from uniaxial tensile tests and also from tear strength tests. These rubbers were then used to form the arterial wall analogue for experimental testing of idealised abdominal aortic aneurysms. These rubber models can be created using previously reported techniques<sup>1,4</sup> for use with videoextensometry. These novel materials could be used to create more physiologically realistic *in vitro* arterial models. The use of a combination of silicones to create a diseased vessel wall could serve as a useful tool in future experimental work.

In particular, these materials could be incorporated into experimental rupture studies to provide more accurate material analogues than those used in previous reports.<sup>2</sup>

## **MATERIALS AND METHODS**

### **Material Selection**

The commercially available Sylgard silicone from Dow Corning was chosen as the base material for this study, in particular, Sylgard 160 and Sylgard 170. Both Sylgards are supplied as a two-part silicone elastomer with Sylgard 160 appearing grey and Sylgard 170 appearing black. These two rubbers are prepared in a 50:50 by weight arrangement, which facilitates mixing and preparation. These silicones were identified as appropriate materials as each material is easily identifiable due to its colour, and importantly, they have dissimilar material properties.

### **Material Development**

Sylgard 160 is naturally grey in appearance with an ultimate tensile strength (UTS) of 4MPa, whereas, Sylgard 170 is naturally black in colour with a UTS value of 2 MPa. These UTS values were obtained from the Dow Corning specification sheets. These two materials were mixed together in various ratios in order to create a range of new silicones, with gradually increasing colour intensity from grey to black and gradually decreasing failure properties from 4-2 MPa. The ratios of each mix were increased by 10% for each new silicone, resulting in 11 complete materials, including the original Sylgard 160 and 170, as shown, for example, in Column I of Table 1.

### **Colour Analysis**

The colour intensity of each silicone was analysed using a ColorLite sph850 Spectrophotometer (ColorLite GmbH). This device allows each silicone mix to be assigned an individual colour intensity value. Colour measurements are given in as a variation of  $\Delta E$ , where pure black has a  $\Delta E$  value of zero. This mathematical model for colour measurement was developed by the Commission Internationale de l'Eclairage (CIE) and is often referred to as the CIELAB formula. The numerical value ( $\Delta E$ ) can be used to differentiate between colours and is given by Equation 1.

$$\Delta E = [\Delta L^2 + \Delta a^2 + \Delta b^2]^{\frac{1}{2}} \quad (1)$$

This equation is based on  $L^*a^*b^*$  values where the lightness value, or luminosity, ( $\Delta L$ ) indicates how light or dark the colour is,  $\Delta a$  represents the position on the red-green axis, and  $\Delta b$  shows the position on the yellow-green axis ( $\Delta b$ ).  $L^*a^*b^*$  values are calculated from the tristimulus values ( $X, Y, Z$ ) which are the backbone of all colour mathematical models. The location of a colour is defined by a three dimensional Cartesian coordinate system which determines the numerical values of  $L^*$ ,  $a^*$  and  $b^*$ , and is shown in Figure 1(A). Once the location of  $L^*a^*b^*$  is determined, a modification of the CIELAB tolerancing is performed, known as CMC tolerancing (Colour Measurement Committee of the society of Dyers and Colourists of Great Britain). This technique mathematically defines an ellipsoid around the standard colour with semi-axis corresponding to hue, chroma, and lightness. Figure 1(B) shows the variation of the ellipse sizes throughout the  $L^*a^*b^*$  colour space. In order to actually determine the  $\Delta E$  value of the particular material, firstly the device is calibrated using a standard colour, in this case the standard reference colour was black. The device is then placed against the material to be tested and allowed to operate. Average colour intensity was recorded from 3 measurements taken for each sample.

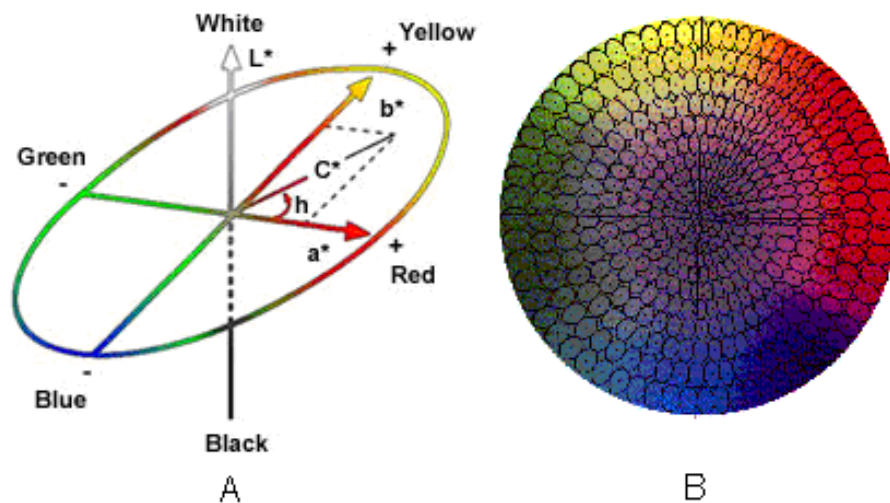


Figure 1: (A) The CIE colour space which defines the location of a particular colour with regards to  $L^*$ ,  $a^*$  and  $b^*$ , and (B) the corresponding ellipse sizes throughout  $L^*a^*b^*$  colour space.

### Uniaxial Tensile Testing

Uniaxial tensile testing was performed using a Tinius Olsen H25KS (Tinius Olsen, Ltd., Surrey RH1 5DZ, England) with a 1 kN load cell. Each material was formed into Type 2 dumb-bell specimens conforming to BS ISO 37. Samples were injected into the dumb-bell shape to eliminate the cutting process, which has to been reported to possibly

lead to poor results.<sup>20</sup> Each sample was subjected to a extension rate of 500 mm/min (BS ISO 37), with a preconditioning of 10 cycles to 20% of the gauge length. Preconditioning helps to increase repeatability of the tests by stabilising the stress-strain function of the material. The structural properties of elastomers change significantly during the first several times that the material experiences straining. This behaviour is commonly referred to as the Mullin's effect.<sup>21</sup> The primary purpose of the tensile testing in this application was to generate force-extension data, which can be converted to stress-strain data, and determine the ultimate tensile strength (UTS) of each silicone mixture.

### **Tear Testing**

Tear testing was performed using a modification of the trouser test pieces outlined in BS ISO 34-1. The Tinius Olsen was again used for this analysis. A strain rate of 100 mm/min was applied to each sample as per BS ISO 34-1. Tear testing results in tear strength (TS) values, which provide an indication of the resistance of the material to tearing, with results given in force per unit length. On failure of the specimen, the tear resistance, or tear strength, is calculated by Equation 2.

$$TS = \frac{F}{t} \quad (2)$$

Where:  $TS$  is the tear strength (N/mm);  $F$  is the maximum load (N); and  $t$  is the specimen thickness (mm).

### **Material Characterisation**

In order to mechanically characterise each material, the experimental force-extension data from the tensile tests were converted to engineering stress and engineering strain. A 2<sup>nd</sup> order polynomial curve was applied to the data to obtain a mean experimental data curve. This mean data was then applied to the commercial finite element analysis (FEA) solver ABAQUS v.6.7 (Dassault Systemes, SIMULIA, RI, USA) in order to find the most applicable strain energy function (SEF), and allow the determination of material coefficients. Material coefficients were then assessed using a Type 2 dumb-bell numerical model. The model was examined using identical boundary conditions to those applied experimentally. The stress and strain at a central node was then mapped throughout the course of the analysis, and compared to the results found experimentally.

### **Calibration Curves**

Once data was compiled from tensile tests, tear tests, and colour analysis, calibration curves could be created. These curves directly relate the colour intensity of the material to a particular UTS and TS, and ultimately, to material properties and material coefficients. For each calibration curve, the  $\Delta E$  value of the material was plotted against both the UTS and TS, with relevant trendlines applied to the data. Error bars represent standard deviation. These linear curves then allow the prediction of material properties depending on the  $\Delta E$  value determined through colour analysis.

### **Effectiveness of Calibration Curves**

In order to examine the accuracy of the calibration curves, a repeated batch of samples were created at each silicone mixture. Each sample was probed with the spectrophotometer to measure the  $\Delta E$  value. Each  $\Delta E$  value relates to both a UTS and TS, thus allowing the UTS and TS to be predicted prior to testing. These samples were then tensile tested and tear tested so as to record both the UTS and TS. The predicted UTS and TS of each material could then be compared to the actual measured value.

### **Idealised AAA Experimental Models**

Idealised AAA silicone models were manufactured. These idealised models were designed to have realistic dimensions based on population averages obtained from the EUROSTAR data registry (2001).<sup>22</sup> The maximum outer diameter of this model is 54 mm. This ideal AAA model has been utilised in previous research by our group.<sup>2,17,23,24</sup> The technique used to create these models has been previously reported.<sup>1,4</sup> Briefly, each silicone model is made using the lost-wax process. An inner wax model is first created using an aluminium mould, which is then placed into a larger mould, consisting of a uniform 2 mm cavity surrounding the wax model. The liquid silicone rubber is then injected into this cavity, and cured. Three models were created using Sylgard 160, three using Sylgard 170, and one model was created by randomly injecting both Sylgard 160 and Sylgard 170 through a Y-tubing connection into the wall cavity. This allowed both silicones to randomly mix via the injection process, resulting in a model of random material properties and various shades of black and grey. These models can be seen in Figure 2.

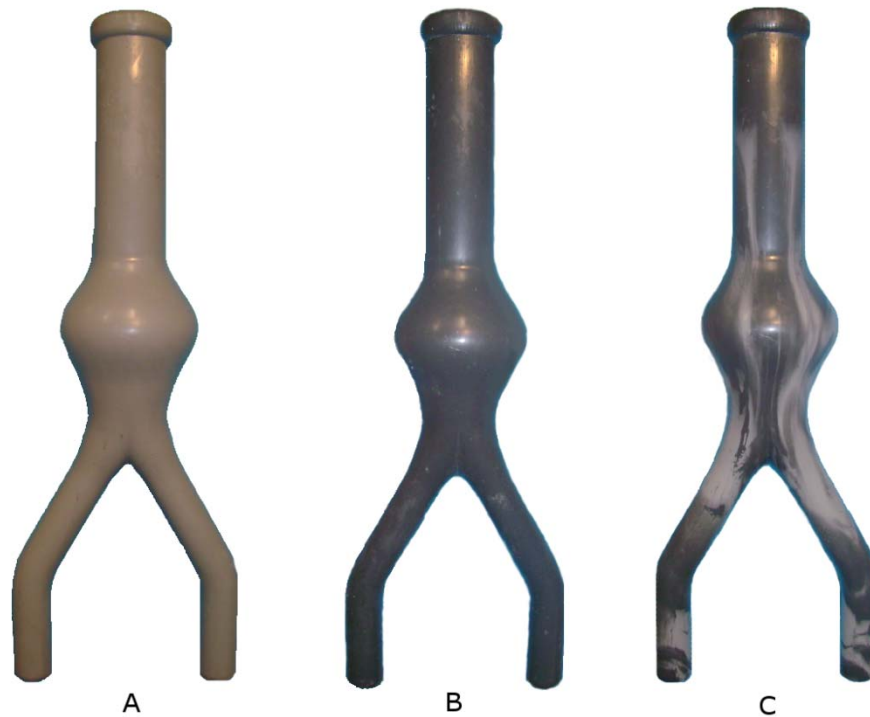


Figure 2: Ideal AAA models created (A) Example Sylgard 160 model, (B) Example Sylgard 170 model and (C) Mixed AAA model.

### **Videoextensometry**

The purpose of this aspect of the study was to examine how the maximum diameter of these silicone models react to increasing pressure loadings, and compare with numerically predicted results using the material coefficients determined earlier. Each model was set-up in the same manner, that is, the model was connected to a pneumatic air source via a pressure regulator and pressure manometer. The iliac legs of each model were blocked and constrained from movement. Applied air pressures were incrementally increased by 20 mmHg from 0-160 mmHg. The diametrical change of each model was recorded with the results then averaged. These measurements were performed with the Messphysik Materials Testing Videoextensometer 1362CA (Messphysik Materials Testing, Austria) in conjunction with the Messphysik Dot Measurement for Windows software.

### **Mixed Model Colour Analysis**

The spectrophotometer was also used to measure the colour intensity of the mixed ideal AAA model of Sylgard 160 and 170. Measurements were taken at 20 mm intervals along the length of the model, at the front, back, left, and right sides. These measurement locations are shown in Figure 3. The readings were taken longitudinally from the start of the proximal neck to end of the iliac legs.

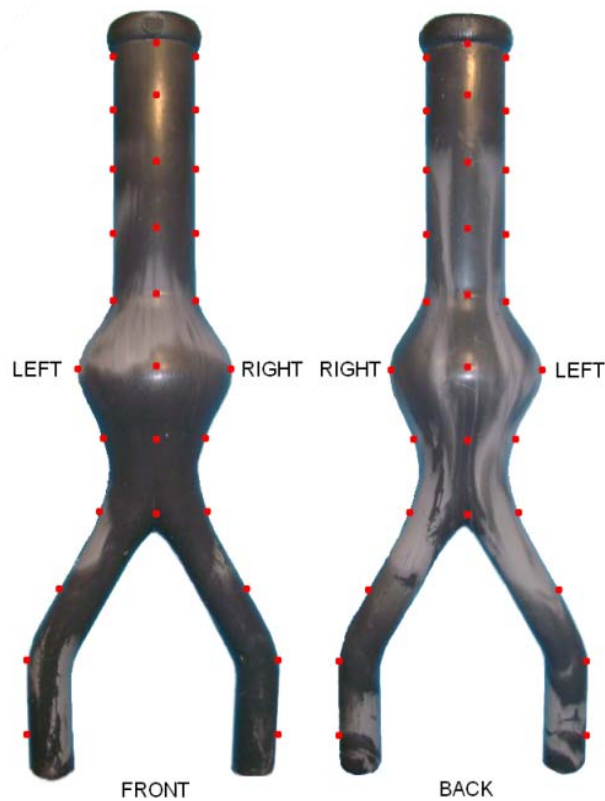


Figure 3: Ideal AAA mixed model created using both Sylgard 160 and Sylgard 170. Red dots indicate locations where colour intensity ( $\Delta E$ ) readings were taken. Distance between dots is 20 mm.

### Statistical Analysis

Significant correlations between results were assessed using a non-parametric Spearman's Rho bivariate correlation test using SPSS 15.0 (SPSS Inc., Chicago, Ill, USA). Correlation coefficient (CC) is shown where significant relationships were observed.

### Numerical Modelling

In order to assess the effectiveness of the material coefficients derived in this study, the videoextensometry experiment was replicated using the finite element method. An identical idealised AAA model was used, which has been used in many previous studies, both experimentally<sup>2,4</sup> and numerically.<sup>23</sup> The numerical model has a uniform wall of 2 mm, and was constrained from movement at the proximal neck and iliac legs, reproducing the experimental set-up. A half model was examined due to the symmetrical nature of the idealised AAA. The model was meshed using 11,443 quadratic tetrahedral 3D stress elements. Mesh independence was achieved by increasing the mesh size until the peak stress was <2% of the previous mesh.<sup>6,16,25</sup> The same loading conditions were applied to the inner surface of the model and the

displacement of the maximum diameter region was measured at each loading. Figure 4 shows the meshed model and also the boundary conditions used. This FEA replication was first modelled as a Sylgard 160 material, then as a Sylgard 170 material, and lastly, with the region of maximum diameter corresponding to the material coefficients determined from the colour analysis. For this mixed material numerical model, a circumferential 10 mm band was partitioned at the region of maximum diameter and assigned material properties corresponding to the  $\Delta E$  value of the region (~Sylgard 160). As the regions from which diameter measurements were to be obtained were all approximately the same  $\Delta E$  value, a circumferential band was deemed to adequately represent the region.

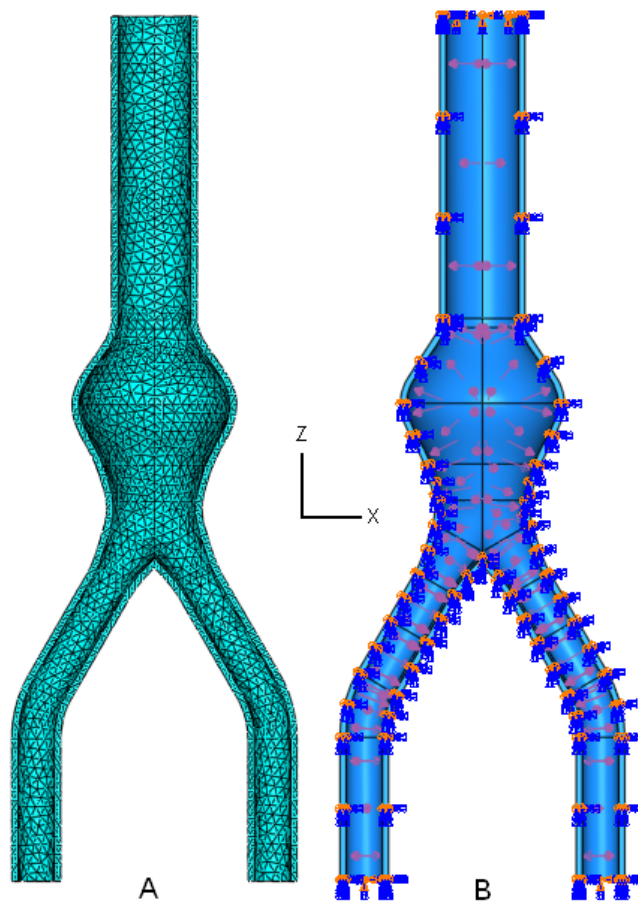


Figure 4: Numerical ideal AAA model used in the analysis. (A) Shows the meshed symmetrical model and (B) illustrates the boundary conditions used. Symmetry constraints were placed along the Y-axis, with the model constrained in all directions at the proximal neck and iliac legs. The pressure loading was applied to the inner surface of the model.

## RESULTS

### Uniaxial Tensile Testing, Tear Testing and Colour Analysis

The results of the experimental uniaxial tensile tests for each silicone mixture can be seen in Table 1, with the results of the tear testing shown in Table 2. These results show the silicone mix ratio, sample size (n), average  $\Delta E$  value, average UTS and average TS. Dow Corning reported the UTS of Sylgard 160 and Sylgard 170 to be 4 MPa and 2 MPa, respectively, although it is known that the upper and lower limits of these values can vary significantly. Good agreement with these reported values were found, with each of the mixes shown to have UTS values within this range. Results from the tear testing show that the TS decreases with respect to the UTS of the material. It was also noted that there was jagged tearing along the direction of the cut in all samples examined for tear strength.

Table 1: Results of the uniaxial tensile testing for each mixture of silicone.  $\Delta E$  and UTS results are mean values of the sample size. Standard deviation (SD) is also shown.

Silicone Type	n	$\Delta E$	SD	UTS (MPa)	SD (MPa)
160	18	47.72	2.57	3.822	0.51
10:90	6	40.16	0.97	3.537	0.498
20:80	6	36.91	0.7	3.599	0.635
30:70	5	31.92	0.95	3.289	0.357
40:60	6	32.52	0.45	2.611	0.33
50:50	12	29.88	0.7	3.206	0.377
60:40	5	27.33	0.39	2.473	0.093
70:30	10	26.41	1.01	2.445	0.279
80:20	5	25.13	0.77	2.199	0.243
90:10	5	24.55	1.21	2.401	0.391
170	20	23.86	1.85	2.077	0.375

Silicone mixes are in ratios of Sylgard 170:Sylgard 160, therefore, 10:90 refers to 1 part Sylgard 170 to 9 parts Sylgard 160

Table 2: Results of the tear testing for each mixture of silicone.  $\Delta E$  and tear Strength results are mean values of the sample size Standard deviation (SD) is also shown.

Silicone Type	n	$\Delta E$	SD	TS (N/mm)	SD (N/mm)
160	6	45.73	0.33	0.697	0.094
10:90	6	40.74	0.22	0.68	0.088
20:80	5	37.23	0.38	0.754	0.079
30:70	6	34.52	0.52	0.692	0.045
40:60	6	31.32	0.58	0.688	0.095
50:50	5	28.54	0.45	0.573	0.034
60:40	6	28.76	0.48	0.537	0.054
70:30	3	26.39	0.14	0.479	0.051
80:20	6	25.40	0.24	0.519	0.069
90:10	6	23.79	0.32	0.433	0.047
170	8	23.84	0.63	0.452	0.049

## Material Characterisation

The stress-strain data generated from tensile testing allowed a SEF to be applied to each material, and therefore, material coefficients to be calculated. A 1<sup>st</sup> order Ogden model was deemed to be the optimum SEF as it provided the most accurate curve fit to the data and also the material remains stable at all stresses and strains. The general Ogden SEF<sup>26</sup> takes the form of Equation 3.

$$W(\lambda_1, \lambda_2, \lambda_3) = \sum_{p=1}^N \frac{\mu_p}{\alpha_p} (\lambda_1^{\alpha_p} + \lambda_2^{\alpha_p} + \lambda_3^{\alpha_p} - 3) \quad (3)$$

Where  $W$  is the strain energy density per undeformed unit volume,  $(\lambda_1, \lambda_2, \lambda_3)$  are the principal stretch ratios,  $\alpha$  is a strain hardening exponent, and  $\mu$  has the interpretation of the shear modulus under infinitesimal straining. By applying this SEF to the experimental data obtained from the tensile tests, material coefficients could be determined. Table 3 shows the  $\mu$  and  $\alpha$  coefficients for each silicone mix examined, with Figure 5 illustrating the effect the silicone mixture has on the resulting  $\mu$  coefficients. The coefficients of each material were then assessed using a comparative Type 2 dumb-bell modelled in ABAQUS v6.7. Results, shown in Figures 6 show the agreement between the stress and strain found experimentally from the tensile tests compared to those determined using FEA for Sylgard 160 and Sylgard 170. Figure 7 shows the good correlation between experimental and numerical results for the new silicone materials.

Table 3: 1<sup>st</sup> order Ogden SEF coefficients for each silicone mixture

Silicone Type	$\Delta E$	$\mu$	$\alpha$
160	46.63	1.6525	3.2395
10:90	40.45	0.7885	3.0366
20:80	37.07	0.7485	2.9704
30:70	33.22	0.6854	2.9807
40:60	31.92	0.5769	2.9243
50:50	29.59	0.5768	2.9278
60:40	28.04	0.5589	2.9286
70:30	26.40	0.5248	2.8296
80:20	25.27	0.4154	3.0707
90:10	24.17	0.3632	3.0265
170	23.82	0.6988	2.9741

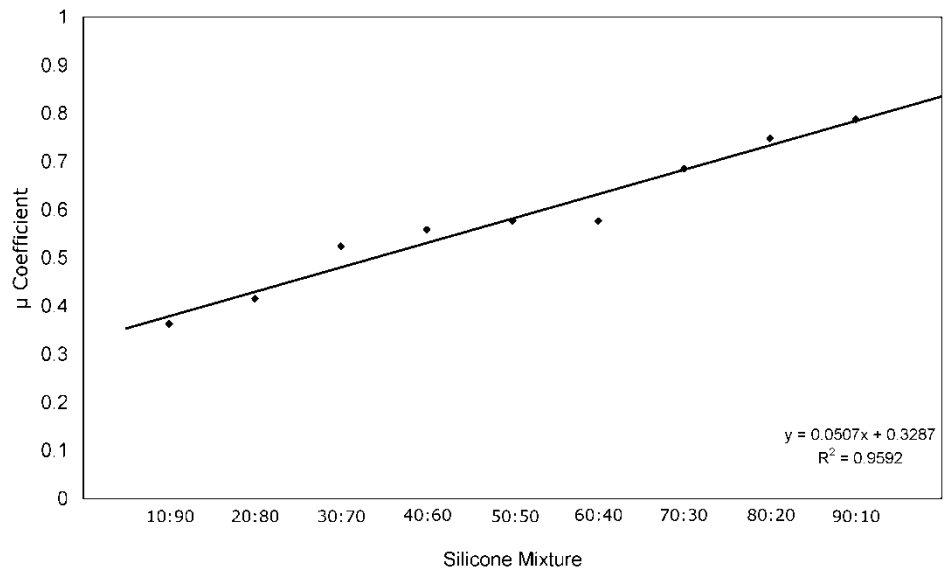


Figure 5: Variation in 1<sup>st</sup> order Ogden  $\mu$  coefficient with differing silicone mixtures.

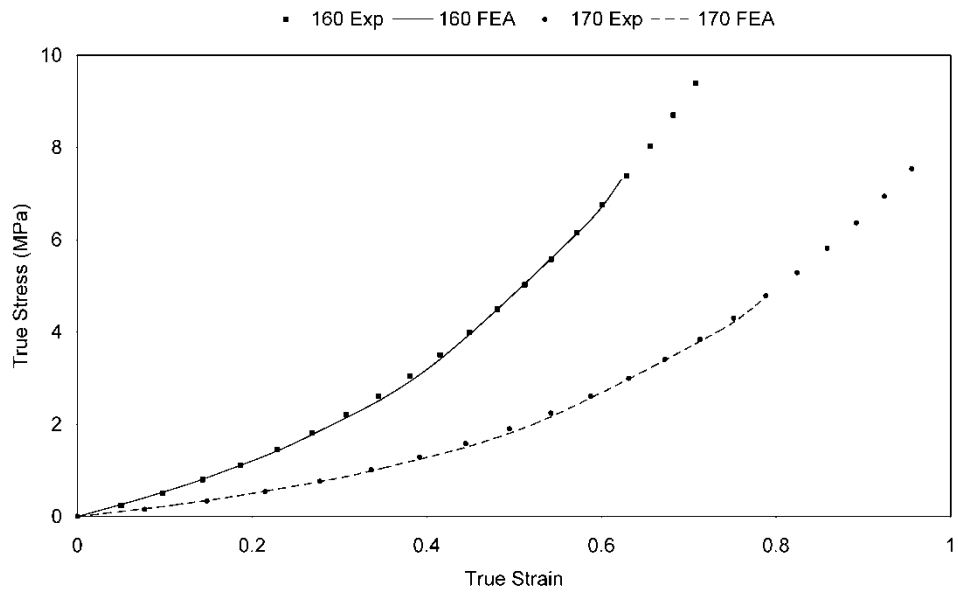


Figure 6: Stress-strain curves for experimental and numerical results for Sylgard 160 and 170.

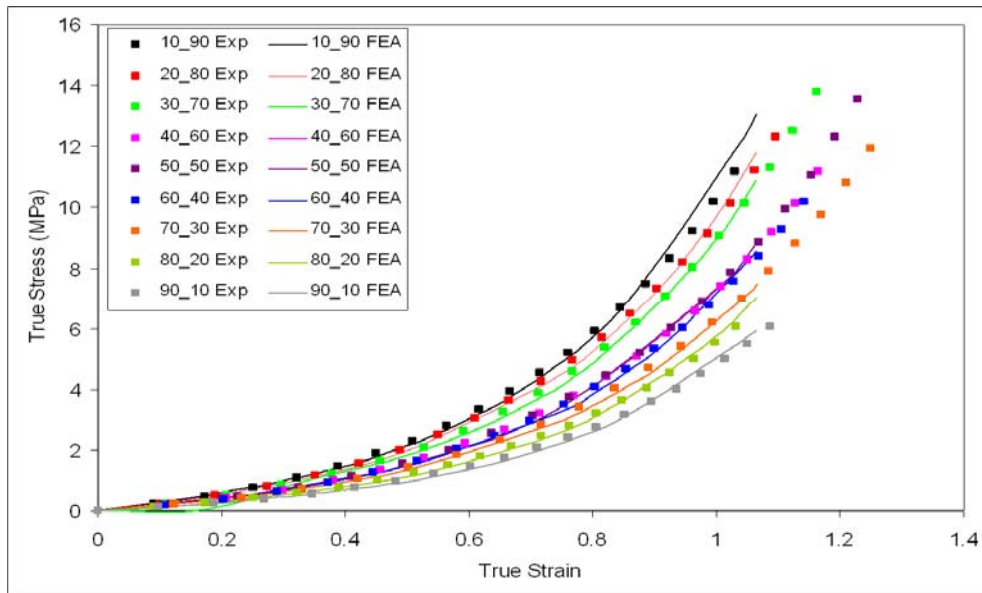


Figure 7: True stress-strain curves for the experimental and numerical results for the new silicone materials.

### Calibration Curves

From the experimental testing and colour intensity measurement, calibration curves could be generated. First, a calibration curve relating  $\Delta E$  to UTS was created, and is shown in Figure 8. Then, a calibration curve relating  $\Delta E$  to TS was generated. This second curve can be seen in Figure 9. The relationship between  $\Delta E$  and both UTS ( $CC=0.955$ ,  $P<0.0009$ ) and TS ( $CC=0.909$ ,  $P<0.0009$ ) were both observed to be significant. Each data point in Figure 8 and 9 is labelled with the corresponding silicone mix ratio of Sylgard 170:Sylgard 160. Good linear relationships were shown between both  $\Delta E$  and UTS ( $R^2=0.8082$ ), and  $\Delta E$  and TS ( $R^2=0.7205$ ).

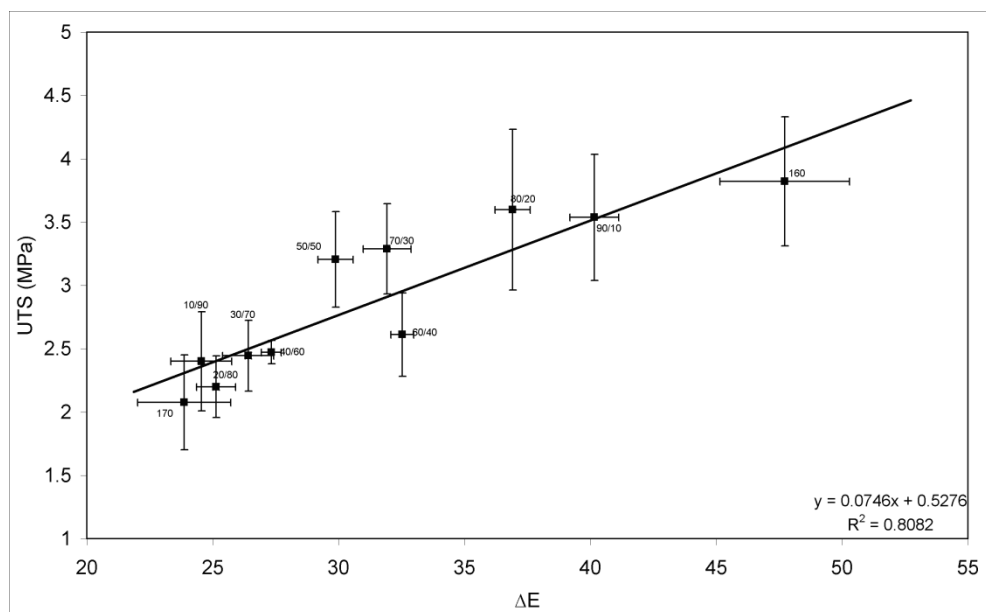


Figure 8: UTS calibration curve for silicones ranging from Sylgard 170 to Sylgard 160.

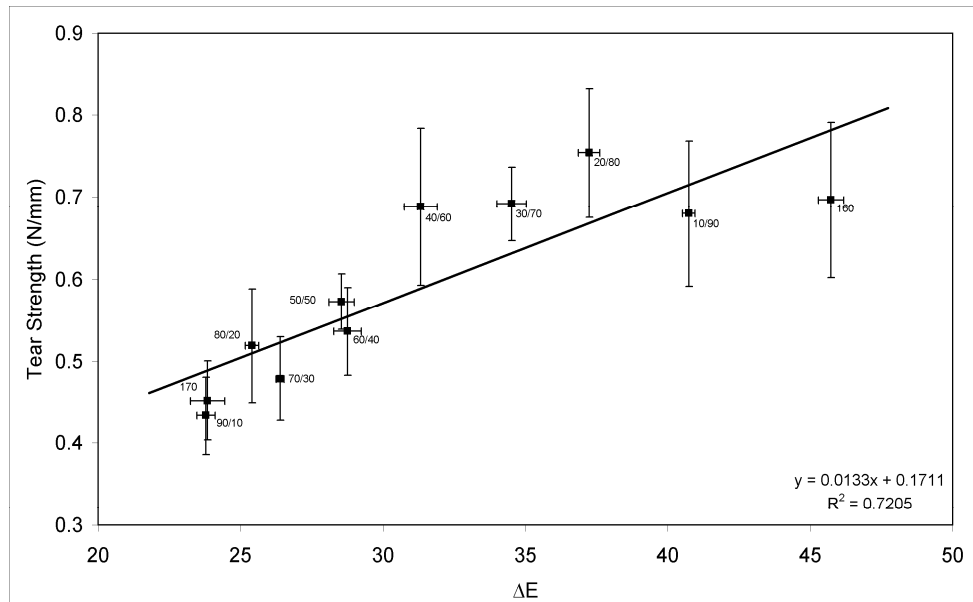


Figure 9: Tear strength calibration curve for silicones ranging from Sylgard 170 to Sylgard 160.

### Effectiveness of Calibration Curves

The accuracy of Figures 8 and 9 were also examined. This was achieved by preparing both dumb-bell and trouser test samples of each silicone mixture and measuring the colour intensity of each sample. This  $\Delta E$  value was then related to UTS using Figure 8 and TS using Figure 9. Dumb-bell samples were then tensile tested, and trouser samples measured for tear strength. The measured UTS and TS of the samples were then compared to the predicted UTS and TS. The results of this test can be seen in Figures 10 and 11. The predicted and measured TS results showed to be significant for the 30:70 ( $CC=0.955$ ,  $P=0.003$ ) and 70:30 mixtures ( $CC=0.851$ ,  $P=0.032$ ). Significance was not observed between the predicted and measured results for other mixes. Good linear agreement was observed between the predicted values and the measured values for both the UTS ( $R^2=0.8556$ ) and the TS ( $R^2=0.8061$ ). Overall, the predicted UTS and measured UTS results were significant ( $CC=0.945$ ,  $P<0.0009$ ), as were the predicted TS and measured TS results ( $CC=0.891$ ,  $P<0.0009$ ).

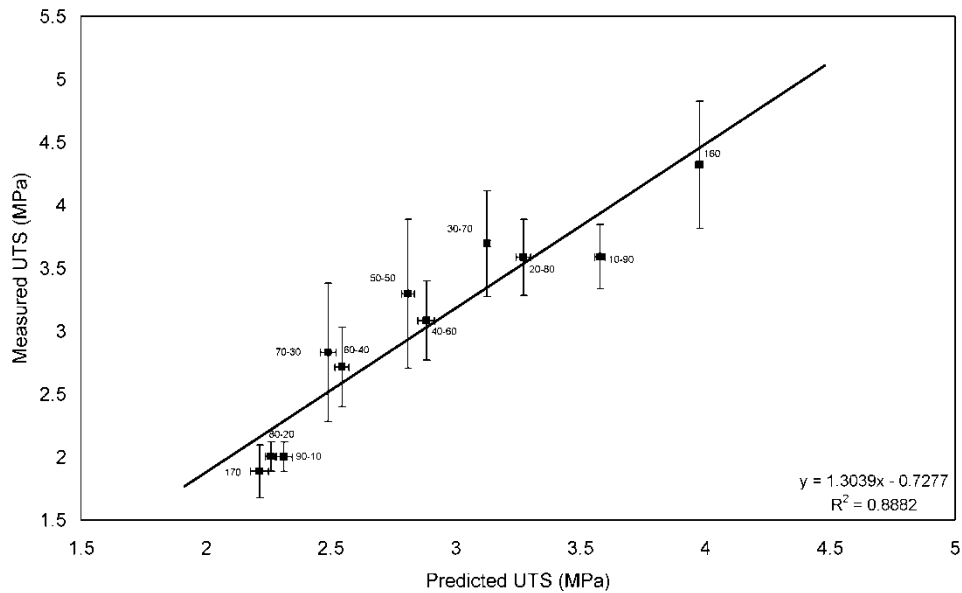


Figure 10: Predicted UTS results compared with those found experimentally for each silicone mixture.

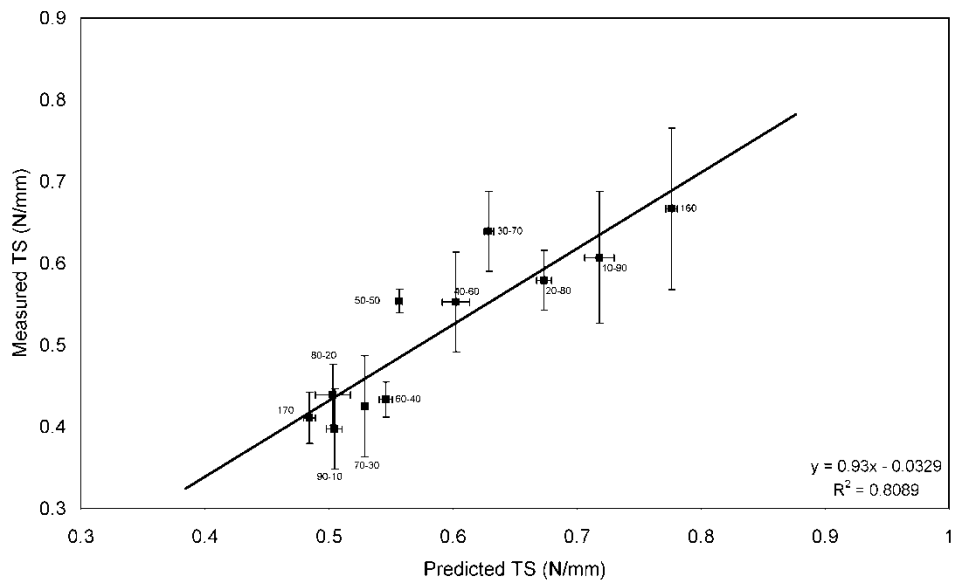


Figure 11: Predicted TS results compared with those found experimentally for each silicone mixture.

### Relationship Between UTS and Tear Strength

The UTS results and tear strength results were also compared resulting in Figure 12, which showed a good linear trend ( $R^2=0.7159$ ) and significant relationship ( $CC=0.9$ ,  $P<0.0009$ ) between the two material properties. This allows tear strength to be related to UTS for each varying silicone material thus giving a further insight into the relationship between the two properties.

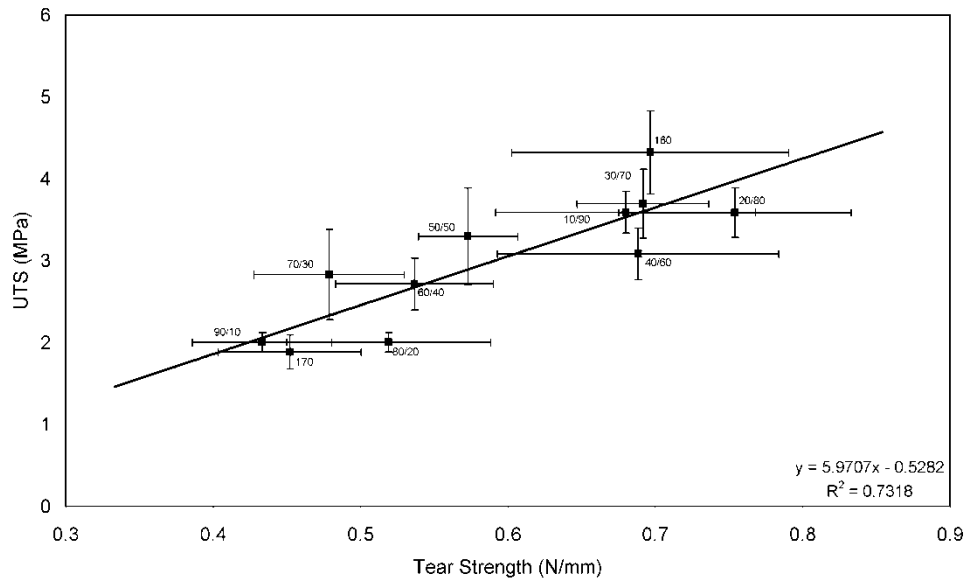


Figure 12: Relationship between tear strength and UTS for each silicone rubber.

### Colour Analysis: Mixed AAA Model

The spectrophotometer was used to determine the  $\Delta E$  value at 20 mm intervals along the longitudinal distance of the model, as shown in Figure 3. The results show how the  $\Delta E$  value differs depending on the concentration of either Sylgard 170 or Sylgard 160. This resulted in a series of colour intensity values corresponding to a specific location on the model, with the values shown in Table 4 and graphically in Figure 13. It can be clearly seen how the colour intensity of the material changes at various locations on the model.

Table 4:  $\Delta E$  measurements at various locations along the length of the ideal AAA mixed model. Measurement locations correspond with Figure 3.

	<b>Front</b>	<b>Back</b>	<b>Left</b>	<b>Right</b>
<b>Distance (mm)</b>	<b><math>\Delta E</math></b>	<b><math>\Delta E</math></b>	<b><math>\Delta E</math></b>	<b><math>\Delta E</math></b>
0	30.38	24.77	31.4	31.58
20	26.02	23.27	28.43	27.25
40	23.94	23.26	29.38	28.07
60	24.07	25.5	28.13	42.98
80	35.09	24.29	27.56	29.91
100	27.45	27.21	45.41	45.31
120	20.12	25.22	39.84	24.42
140	23.16	27.56	44.04	33.41
160	-	-	45.13	45.41
180	-	-	26.99	26.85
200	-	-	27.52	36.93
220	-	-	30.11	30.94

*Note:* Front and back do not have  $\Delta E$  values past 140mm due to the geometry of the model.

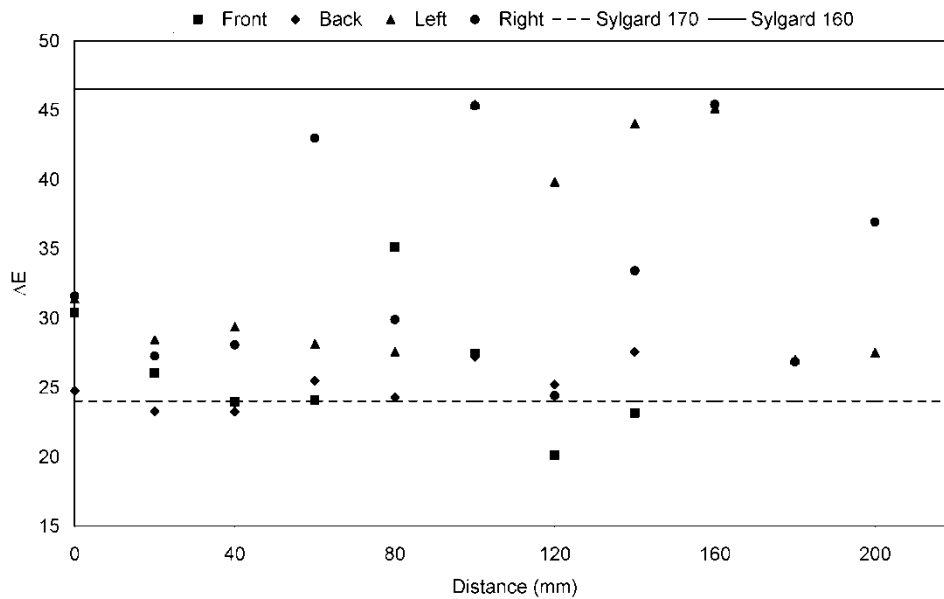


Figure 13:  $\Delta E$  variation along the longitudinal distance of the ideal AAA mixed model.

### Videotensometry

As the air pressure was incrementally increased, the diametrical change of each model was measured and recorded. The initial maximum diameter of each model was 54 mm, and so any displacement past 54 mm at each pressure loading is recorded with the software. Tables 5, 6 and 7 show the results of the experimental pressure-diameter testing, with the results summarised graphically in Figure 14.

Table 5: Pressure-diameter results for the Sylgard 160 ideal AAA models. Each set of results for each model is a combination of measurements taken from both the front and side

Pressure (mmHg)	Model 1	Model 2	Model 3	Average (mm)
0	54	54	54	54
20	54.01	54.01	54.02	54.01
40	54.02	54.02	54.05	54.03
60	54.04	54.03	54.07	54.05
80	54.08	54.06	54.09	54.07
100	54.13	54.09	54.11	54.11
120	54.18	54.13	54.15	54.15
140	54.23	54.17	54.19	54.19
160	54.27	54.22	54.23	54.24

Table 6: Pressure-diameter results for the Sylgard 170 ideal AAA models. Each set of results for each model is a combination of measurements taken from both the front and side

<b>Pressure (mmHg)</b>	<b>Model 1</b>	<b>Model 2</b>	<b>Model 3</b>	<b>Average (mm)</b>
0	54	54	54	54
20	54.07	54.04	54.04	54.05
40	54.14	54.09	54.12	54.12
60	54.23	54.16	54.19	54.19
80	54.39	54.30	54.32	54.33
100	54.54	54.41	54.47	54.47
120	54.71	54.66	54.66	54.67
140	54.92	54.86	54.86	54.88
160	55.10	55.05	55.06	55.07

Table 7: Pressure-diameter results for the randomly-mixed ideal AAA model.

<b>Pressure (mmHg)</b>	<b>Diameter (mm)</b>
0	54
20	54.00
40	54.01
60	54.06
80	54.20
100	54.32
120	54.51
140	54.67
160	54.83

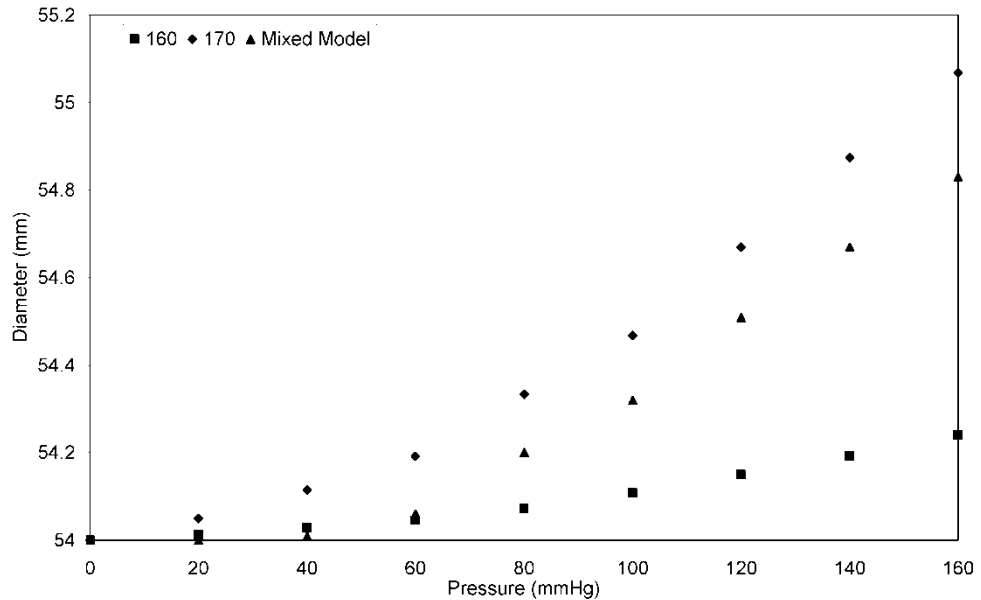


Figure 14: Pressure-diameter results for the Sylgard 160, Sylgard 170 and mixed ideal AAA models.

### Numerical Modelling

By measuring the displacement at the region of maximum diameter, the deformation of the experimental models could be compared to those observed numerically. The experimental and numerical results were statistically significant for the Sylgard 160

model ( $CC=1.0$ ,  $P<0.0009$ ), Sylgard 170 model ( $CC=1.0$ ,  $P<0.0009$ ) and also the mixed silicone model ( $CC=0.971$ ,  $P<0.0009$ ). Overall, there was a difference in the diameter change of 0.24% (range 0.01-1.78%) and 0.38% (range 0.3-5.27%) for the Sylgard 160 and Sylgard 170, respectively. For the mixed ideal AAA model, deformations were only measured from the front of the model, as with the experimental model, with an average percentage difference of 0.76% (range 0.25-5.03%). The results can be seen tabulated in Table 8 and graphically in Figure 15.

Table 8: Summarised results comparing diameter changes between those found experimentally and numerically. All dimensions are maximum diameter and are given in millimetres (mm).

Pressure (mmHg)	Sylgard 160		Sylgard 170		Mixed Model	
	Experimental	FEA	Experimental	FEA	Experimental	FEA
0	54	54	54	54	54	54
20	54.012	54.030	54.050	54.040	54.000	54.035
40	54.028	54.039	54.115	54.084	54.010	54.007
60	54.045	54.040	54.192	54.189	54.060	54.085
80	54.073	54.059	54.333	54.325	54.200	54.188
100	54.108	54.095	54.468	54.487	54.320	54.314
120	54.150	54.138	54.670	54.673	54.510	54.460
140	54.192	54.186	54.875	54.885	54.670	54.629
160	54.240	54.240	55.068	55.121	54.830	54.813

Note: Experimental and FEA results for all three analyses were significant at the 0.05 level

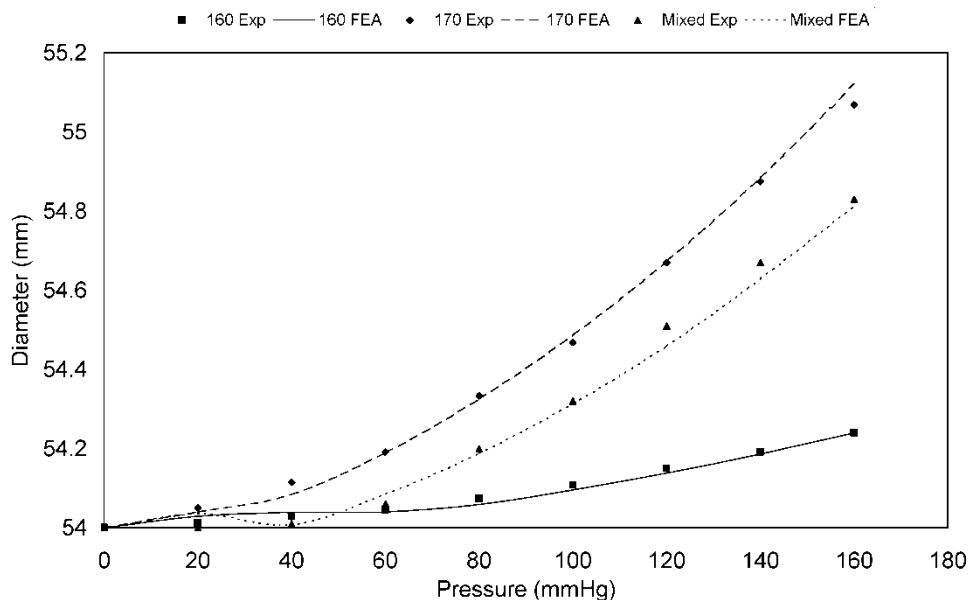


Figure 15: Comparison of results for maximum diameter change with increased pressure loading for both the experimental (Exp) and FEA results.

## **DISCUSSION**

### **Material Development**

Silicone rubbers are widely used as arterial analogues in experimental studies.<sup>1-4</sup> When utilising silicone in experimental testing, a complete understanding of the mechanical behaviour of the material is important in order to correctly measure and assess results. The purpose of this study was to design a number of silicones with a distinct range of material properties and utilise these materials as improved arterial analogues. It was also necessary to be able to identify and correlate material variations non-destructively, as it was essential that material properties could be determined without further experimental testing. The results presented suggest that the range of silicones developed could be readily implemented in future *in vitro* studies providing models with predictable non-uniform material properties that are more representative of the behaviour of arterial tissue. In order to develop the range of silicone rubbers presented, base materials were required. The materials chosen were Sylgard 160 and Sylgard 170 from the Dow Corning range of silicone rubbers. These materials were selected due to their relatively low UTS values of 4 MPa and 2 MPa, respectively, and also due to their natural appearance, that is, Sylgard 160 is grey and Sylgard 170 is black in colour. These strength values are slightly outside the range of tensile strengths of AAA tissue previously reported: 0.38-0.73 MPa;<sup>27</sup> 0.864 MPa;<sup>28</sup> 0.336-2.351 MPa.<sup>19</sup> However, as AAA tissue does experience a range of tensile strengths, the repeatable nature of this developed range can be employed to create distributions of strengths, thus making the range somewhat comparable to the realistic setting.

### **Colour Analysis**

A result of these various mixes was that each new material had a differing appearance, with the colour slightly changing from grey to black as the mix ratio increased from pure Sylgard 160 to Sylgard 170. This change in physical appearance of each new silicone facilitated the analysis of each material using a non-destructive method of determining colour intensity. Colour intensities were measured using a spectrophotometer. This device measures the colour intensity based on the lightness, chroma and hue of the particular material. The  $\Delta E$  value proved to be a repeatable method of determining colour intensities between the various materials, with the results shown in Tables 1 and 2. Slight deviations exist between  $\Delta E$  values for the same material, yet overall the method is robust, showing a linear increase in  $\Delta E$  as the material changes from black (Sylgard 170) to grey (Sylgard 160).

## Material Characterisation

Once the colour analysis was determined, it was necessary to mechanically characterise the range of materials. This was performed by uniaxially tensile testing and tear testing each silicone rubber to assess, firstly, the UTS of each material, and secondly, the tear resistance, or tear strength (TS), of each rubber. Tensile testing and tear testing was performed according to BS ISO 37 and BS ISO 34-1 standards, respectively. The tensile testing generated force-extension curves, which were converted to engineering stress and strain data. The tear testing records the peak force required to tear the sample and then divides this by the sample thickness. This results in tear strength values given in N/mm. UTS values for each material ranged from 2.077-3.822 MPa, values of which lie within the reported UTS values for Sylgard 170 and Sylgard 160 (2-4 MPa) according to the Dow Corning specification sheet. These results show that the UTS values have a linear relationship with silicone type (see Table 1), which was the desired outcome. Tear testing was performed on trouser test pieces, modified from the sample described in BS ISO 34-1. Again, tear testing revealed that the TS has a linear relationship with silicone type (See Table 2), with values ranging from 0.452-0.697 N/mm. These values are lower than those supplied on the Dow Corning data sheet and are not comparable, as it is known that tear strengths depended heavily on the type of specimen used in the testing.<sup>29</sup>

Applying the data obtained from the experimental testing to the numerical solver allowed the 1<sup>st</sup> order Ogden SEF to be deemed the most suitable SEF. ABAQUS v6.7 then generates material coefficients for the 1<sup>st</sup> order Ogden SEF that accurately represent each material. These material coefficients can be seen in Table 3. The resulting change in  $\mu$  coefficient for each mixture can be seen in Figure 5. As Sylgard 160 and Sylgard 170 were designed by Dow Corning and never intended to be mixed together, the actual mixing of these material may cause an unusual reaction within the polymerisation of the materials, and this had to be investigated. As a result of this, the pure Sylgards 160 and 170 are homogenous materials, whereas the new materials may be inhomogeneous. The homogenous Sylgards have coefficients that do not conform to the linear trend displayed in Figure 5, whereas, the nine other inhomogeneous mixtures designed in this study are new materials and the coefficients vary linearly depending on the mix ratio. It was determined that when numerically modelling any of the developed silicones, the material coefficients can be implemented with the 1<sup>st</sup> order Ogden SEF within the FEA software. A numerical model of the dumb-bell was analysed in

ABAQUS v6.7 using the coefficients determined earlier and by applying identical boundary conditions to those employed experimentally. This was achieved by plotting the stress and strain at a central node in model throughout the loading. Results of this analysis agreed well with the experimental results for each of the eleven materials examined, as shown in Figures 6 and 7.

The next stage in the study was to develop calibration curves for the range of silicones. These curves allow the use of a silicone rubber to be assessed for colour intensity prior to mechanical testing. The resulting  $\Delta E$  value can then be related to a UTS and TS, allowing the determination of material property through non-destructive testing. The calibration curves for both the  $\Delta E$ -UTS and  $\Delta E$ -TS relationships can be seen in Figures 8 and 9, respectively. The calibration curves for  $\Delta E$ -UTS ( $R^2=0.8082$ ,  $CC=0.955$ ,  $P<0.0009$ ) and  $\Delta E$ -TS ( $R^2=0.7205$ ,  $CC=0.909$ ,  $P<0.0009$ ) were observed to have strong linear, significant relationships. The effectiveness of these curves was also examined. This was achieved by creating a duplicate batch of dumb-bell and trouser samples, and then measuring the  $\Delta E$  value of each sample. The material property of the particular specimen could then be pre-determined using Figures 8 and 9 prior to testing. Tensile and tear testing of the sample then revealed the actual measured UTS and TS of the sample. Figures 10 and 11 show how these predicted values compared to those measured experimentally. For both the UTS and TS, the values predicted using the calibration curves agreed well with those determined from further testing. The predicted TS and measured TS for the 30:70 mixture ( $CC=0.955$ ,  $P=0.003$ ) and the 70:30 ( $CC=0.851$ ,  $P=0.032$ ) mixture were the only materials to exhibit statistical significance. This may be due to the relatively low sample sizes for each mixture. It is believed that by increasing the sample sizes may lead to significance of results. Figures 10 and 11 also show the good linear relationships between both the predicted and measured UTS values ( $R^2=0.8556$ ,  $CC=0.945$ ,  $P<0.0009$ ) and the predicted and measured TS values ( $R^2=0.8061$ ,  $CC=0.891$ ,  $P<0.0009$ ). It was now possible to relate the UTS with the TS for the range of silicones. These results can be seen in Figure 12 and also displayed statistical significance ( $R^2=0.7159$ ,  $CC=0.9$ ,  $P<0.0009$ ). As a result, *in vitro* silicone models with varying material properties can now be created and the distribution of varying material properties can be determined using non-destructive testing.

### **Ideal AAA Models**

The next aspect of this work focused on applying the methodology developed to more appropriate geometries by creating silicone models of an idealised abdominal aortic aneurysm (AAA) model. These models were created using the lost-wax process, and form an idealised AAA model of silicone rubber with a wall thickness of 2 mm. It has been reported that slight deviations can exist in the uniformity of the wall but within acceptable tolerances.<sup>1,4</sup> Three models of Sylgard 160 and three of Sylgard 170 were manufactured, with one further model created using a combination of the two materials injected through a Y-tubing connection. These models can be seen in Figure 2. The mixed model therefore consists of a random mixture of Sylgard 160 and 170 throughout the model, and thus has a random distribution of varying material properties within the ranges presented. The models were then used to evaluate the methodology (of non-destructively determining a varying material property distribution) described earlier.

Firstly, the mixed model was examined using the spectrophotometer. As the model had a random distribution of material mixtures, and therefore a random distribution of differing shades of black and grey, it was expected that the  $\Delta E$  value would vary at different locations on the model. The  $\Delta E$  value was measured at 20mm intervals along the longitudinal distance of the model, at the front, back, left and right sides. The results of this are shown in Table 4 and Figure 13. By comparing Figures 3 and 13, it can be clearly seen how the  $\Delta E$  value varies according to the location on the model. This analysis allows the  $\Delta E$  value at a specific region to be related to a material property, and also to a set of coefficients to be used with the 1<sup>st</sup> order Ogden SEF. For example, in the case of the mixed model, the  $\Delta E$  value at the left and right sides of the maximum diameter region were 45.41 and 45.31, respectively. These values correspond with 1<sup>st</sup> order Ogden  $\mu$  and  $\alpha$  coefficients of 1.6525 and 3.2395 from Table 3.

### **Videoextensometry**

The results of the videoextensometry work can be seen in Tables 5-7 and also in Figure 14. The change in stiffness between the various materials can be clearly seen. Sylgard 160 is stiffer than Sylgard 170, and this can be seen by the minor change in maximum diameter, even at high pressures of 160 mmHg. At this elevated pressure the maximum diameter of the Sylgard 160 deformed by 0.24 mm, compared with a 1.068 mm diameter change for the Sylgard 170 models. Figure 14 also shows how the mixed

model performed. This model was a combination of Sylgard 160 and 170, and therefore, the pressure-diameter results lay in between those of the two Sylgard materials. The maximum diameter of this model had a  $\Delta E$  value of approximately 45, and so was predominately Sylgard 160, hence the mixed model experienced a maximum diameter change similar to that of the pure Sylgard 160 model (0.83 mm vs. 1.068 mm).

### **Numerical Validation**

Identical boundary conditions to those used experimentally were applied to the numerical model, using the material coefficients derived earlier. The numerical model complete with boundary conditions can be seen in Figure 4. A static pressure was applied to the internal surface of the model, with the displacements of the maximum diameter region recorded at each pressure loading. This analysis was performed for a pure Sylgard 160, pure Sylgard 170, and the mixed model, as with the experimental testing. Table 8 and Figure 15 show how these experimental and numerical results compared.

For both the Sylgard 160 and Sylgard 170 models, the percentage difference between the experimental and numerical results was 0.24% (range 0.01-1.78%) and 0.38% (range 0.3-5.27%), respectively. There was also significance observed in the validation of experimental and numerical results for both the Sylgard 160 models ( $CC=1.0$ ,  $P<0.0009$ ) and the Sylgard 170 models ( $CC=1.0$ ,  $P<0.0009$ ). When analysing the mixed AAA model, the colour analysis of the mixed silicone model revealed that the left and right side of the maximum diameter region had a  $\Delta E$  value very close to that of pure Sylgard 160. In order to replicate the mixed model, which has a random array of material properties in the AAA wall, a 10mm circumferential band was created at the region of maximum diameter. The model was analysed with a circumferential band, as the regions at the maximum diameter from which the experimental results were obtained had very similar  $\Delta E$  values (left=45.41, right=45.31) and therefore it was assumed that the region was essentially the same material. Results of this examination show that the experimental and numerical deformations agree well, with an overall percentage difference of 0.76% (range 0.25-5.03%). Significance was also noted with these results ( $CC=0.971$ ,  $P<0.0009$ ). These percentage differences observed for all models were calculated from Table 7 and are within acceptable limits, as the maximum percentage difference of 5.27% recorded in the Sylgard 170 model, only relates to a

difference in diameter of 55.07 mm compared to 55.12 mm, that is, a percentage difference equal to 0.05 mm.

Further to previous reports on rubber model creation,<sup>1,4</sup> methods of including calcification analogues into the AAA wall are possible. Calcifications have been shown to alter the wall stress distributions in numerical models<sup>30</sup> and so the examination of these calcified deposits within *in vitro* models may yield interesting results. These calcification analogues could also be characterised and calibrated to material properties using the methods described here, thus creating an even more realistic experimental model. Also, the materials and methods described here are not limited to AAAs. Lethal aneurysms also form in the cerebral arteries and the thoracic aorta, and as with ongoing research into AAAs, there is a need to develop more realistic *in vitro* models of these aneurysms to further understand the biomechanical behaviour of these diseased vessels. Therefore, there is a need to develop a method of creating experimental AAA models with known material properties that can be determined using a non-destructive method.

### **Limitations**

It is known that there are many available techniques to mechanically characterise silicone rubbers, such as biaxial and equibiaxial tensile testing, and compression testing. It is believed that although these tests were not performed in this study, future work with these experiments may further enhance the material characterisation presented here. Deviations still exist within the UTS and TS results for the rubbers. Increasing the sample sizes used for each variation of silicone may help reduce these errors. Although, with regards to material UTS, Dow Corning state that the upper and lower limits of UTS values for silicones can vary significantly as silicone rubbers are not usually designed to fail. It is often simply the stress-strain response that is of paramount concern, and not the UTS, depending on the application. Also, the percentage differences, although quite small, observed in the videoextensometry compared to the numerical models could be reduced. It is known that slight variations in wall thickness exist within the silicone models, and the use of computed tomography (CT) scanning of the rubber model prior to testing may help eliminate this. CT scan data of each model could be reconstructed using available 3D reconstruction techniques and imported to FEA software for analysis. This would allow an experimentally accurate model to be analysed numerically, instead of the perfectly uniform wall model employed in this study. Also, modelling the mixed silicone model numerically could be improved by

creating a “marbled” numerical model similar to that in experimental testing, instead of the “banded” model examined here. These issues will be addressed in future studies.

## **CONCLUSIONS**

This study has successfully designed and developed a range of silicone rubbers that are not only visually different and easily detectable using a spectrophotometer, but also have a range of material properties that correlate to the visual appearance. The spectrophotometer proved to be effective in differentiating between the various shades of colour. Extensive experimental testing and colour intensity analyses lead to the development of calibration curves relating colour to both UTS and TS. Material characterisation was also performed resulting in a complete set of material coefficients for each of the new silicone rubbers. Testing also showed that the calibration curves are effective in predicting the material properties. Experimental AAA models of known and random material properties were also created. Pressure-diameter experiments and numerical modelling showed that the material coefficients accurately describe the behaviour of the silicone rubber, with minimal percentage differences. Future experimental studies could include these materials, with the material coefficients readily available to be incorporated into any finite element solver.

## **ACKNOWLEDGEMENTS**

The authors would like to thank our funding sources (i) the Irish Research Council for Science, Engineering and Technology (IRCSET) Grant RS/2005/340 and (ii) Grant #R01-HL-060670 from the US National Heart Lung and Blood Institute. The authors would also like to thank the contribution of Joseph Muthu, Departments of Surgery and Bioengineering, Centre for Vascular Remodelling and Regeneration, University of Pittsburgh, USA.

## **REFERENCES**

1. Doyle BJ, Morris LG, Callanan A, Kelly P, Vorp DA, McGloughlin TM. 3D reconstruction and manufacture of real abdominal aortic aneurysms: From CT scan to silicone model. *J Biomech Eng* 2008;130:034501-5.
2. Doyle BJ, Corbett TJ, Callanan A, Walsh, MT, Vorp DA, McGloughlin TM. An experimental and numerical comparison of the rupture locations of an abdominal aortic aneurysm. *J Endovasc Ther* 2009;16:322-335.
3. Marins PALS, Natal Jorge RM, Ferreira AJM. A comparative study of several material models for prediction of hyperelastic properties: Application to silicone-rubber and soft tissues. *Strain* 2006;42:135-47.

4. O'Brien T, Morris L, O'Donnell M, Walsh M, McGloughlin TM. Injection-moulded models of major and minor arteries: The variability of model wall thickness owing to casting technique. *Proc IMechE Part H: J Eng Med* 2005;219:381-6.
5. Shergold OA, Fleck NA, Radford D. The uniaxial stress versus strain response of pig skin and silicone rubber at low and high strain rates. *Int J Impact Eng* 2006;32:1384-1402.
6. Doyle BJ, Callanan A, McGloughlin TM. A comparison of modelling techniques for computing wall stress in abdominal aortic aneurysms. *Biomed Eng Online* 2007;6:38.
7. Doyle BJ, Callanan A, Burke PE, Grace PA, Walsh MT, Vorp DA, McGloughlin TM. Vessel asymmetry as an additional diagnostic tool for the assessment of abdominal aortic aneurysms. *J Vasc Surg* 2009;49:443-454.
8. Doyle BJ, Callanan A, Walsh MT, Grace PA, McGloughlin TM. A finite element analysis rupture index (FEARI) as an additional tool for abdominal aortic aneurysm burst prediction. *Vasc Dis Prev* 2009;6:114-121.
9. Fillinger MF, Raghavan ML, Marra SP, Cronenwett JL, Kennedy FE. In vivo analysis of mechanical wall stress and abdominal aortic aneurysm rupture risk. *J Vasc Surg* 2002;36:589-97.
10. Fillinger MF, Marra SP, Raghavan ML, Kennedy FE. Prediction of rupture risk in abdominal aortic aneurysm during observation: wall stress versus diameter. *J Vasc Surg* 2003;37:724-32.
11. Nicholls SC, Gardner JB, Meissner MH, Johansen HK. Rupture in small abdominal aortic aneurysms. *J Vasc Surg* 1998;28:884-8.
12. Raghavan ML, Vorp DA, Federle MP, Makaroun MS, Webster MW. Wall stress distribution on three-dimensionally reconstructed models of human abdominal aortic aneurysm. *J Vasc Surg* 2000;31:760-9.
13. Thubrikar MJ, Al-Soudi J, Robicsek F. Wall stress studies of abdominal aortic aneurysm in a clinical model. *Ann Vasc Surg* 2001;15:355-66.
14. Venkatasubramaniam AK, Fagan MJ, Mehta T, Mylankal KJ, Ray B, Kuhan G, Chetter IC, McCollum PT. A comparative study of aortic wall stress using finite element analysis for ruptured and non-ruptured abdominal aortic aneurysms. *Eur J Vasc Endovasc Surg* 2004;28:168-76.
15. Vorp DA, Raghavan ML, Webster MW. Mechanical wall stress in abdominal aortic aneurysm: influence of diameter and asymmetry. *J Vasc Surg* 1998;27(4):632-9.
16. Wang DHJ, Makaroun MS, Webster MW, Vorp DA. Effect of intraluminal thrombus on wall stress in patient-specific models of abdominal aortic aneurysm. *J Vasc Surg* 2002;36:598-604.
17. Morris L, O'Donnell P, Delassus P, McGloughlin T. Experimental assessment of stress patterns in abdominal aortic aneurysms using the photoelastic method. *Strain* 2005;40:165-72.
18. Flora HS, Talie-Faz B, Ansdell L, Chaloner EJ, Sweeny A, Grass A, Adiseshiah M. Aneurysm wall stress and tendency to rupture are features of physical wall properties: An experimental study. *J Endovasc Ther* 2002;9:665-75.
19. Raghavan ML, Kratzberg J, de Tolosa EMC, Hanaoka MM, Walter P, da Silva ES. Regional distribution of wall thickness and failure properties of human abdominal aortic aneurysm. *J Biomech* 2006;39(16):3010-6.
20. Feger C. Mechanical testing of thin polymer films. In: *Proceedings of the 4<sup>th</sup> International Symposium on Advanced Packaging Materials*. 1998;pp.77-81.
21. Mullins L. Softening of rubber by deformation. *Rubber Chem Technol* 1969;42:339-62.

22. EUROSTAR Data Registry Centre. Laheij R, van Marrewijk C, Buth J. Progress report on the procedural and follow up results of 3413 patients who received stent graft treatment for infrarenal aortic aneurysms for a period of 6 years. 2001
23. Callanan A, Morris LG, McGloughlin TM. Numerical and experimental analysis of an idealised abdominal aortic aneurysm. European Society of Biomechanics, S-Hertogenbosch, Netherlands 2004.
24. O' Brien T P, Walsh M T, Morris L G, Grace P A, Kavanagh E G, McGloughlin T M. Numerical and Experimental Techniques for the Study of Biomechanics in the Arterial System. In: Leondes CT (ed) Biomechanical Systems Technology, World Scientific Publishing Co., Singapore, 2008;Chap 7:233-70.
25. Truijers M, Pol JA, SchultzeKool LJ, van Sterkenburg SM, Fillinger MF, Blankensteijn JD. Wall stress analysis in small asymptomatic, symptomatic and ruptured abdominal aortic aneurysms. *Eur J Vasc Endovasc Surg* 2007;33:401-7.
26. Ogden RW. Nonlinear elastic deformations. Dover Publication Inc., Mineola, NY, USA. 1984
27. Thubrikar MJ, Labrosse M, Robicsek F, Al-Soudi J, Fowler B. Mechanical properties of abdominal aortic aneurysm wall. *J Med Eng Technol* 2001;25(4):133-42.
28. Raghavan ML, Webster MW, Vorp DA. Ex vivo biomechanical behaviour of abdominal aortic aneurysm: assessment using a new mathematical model. *Ann Biomed Eng* 1996;24:573-82.
29. Brown R. Physical testing of rubber. 4<sup>th</sup> Ed. Springer Science+Business+Media, Inc., NY, USA. 2006;159-67.
30. Speelman L, Bohra A, Bosboom EMH, Schurink GWH, van de Vosse FN, Makaroun MS, Vorp DA. Effects of wall calcifications in patient-specific wall stress analyses of abdominal aortic aneurysms. *J Biomech Eng* 2008;129:105-9.